Progress In Electromagnetics Research C, Vol. 104, 99–113, 2020

Reduction of Cogging Torque and Improvement of Electrical Parameters in Axial Flux Permanent Magnet (AFPM) Synchronous Generator with Experimental Verification

Engin Hüner* **and Gökhan Zeka**

Abstract—This paper presents an axial flux permanent magnet (AFPM) synchronous generator that was manufactured for the reduction of cogging torque by considering the different angles of a rectangle-shaped permanent magnet (RSPM). The placement angle of RSPM was changed from 0 to 28 degrees to obtain total harmonic distortion, line voltage, and cogging torque. A numerical finite element model using Maxwell software was created. The model was validated by the experimental results, with and without a load. The optimum placement angle was obtained at 20 degrees, whose total harmonic distortion (Thd) and cogging torque (Tc) were improved by 41.6% and 71.4%, respectively.

1. INTRODUCTION

In recent years, global warming is the most important problem for the environment. Studies in the literature have shown that fossil fuel consumption is the most important reason. The global warming and energy crisis have caused increased need for renewable energy technologies [1].

One of the renewable energy sources is wind energy. The mechanical energy produced by wind energy was first used in sails. The first wind turbine was seen in windmills. Nowadays, questions on the reliability of nuclear energy have led to a shift toward interesting renewable energy sources. A wind turbine consists of rotor blades, a reduction gear system for changing the speed, a generator supplying the voltage, and a converter for providing regulating voltage. NdFeB magnets have high magnetic density. Therefore, NdFeB is used as a permanent magnet (PM) in generators. The generators with PM are divided into radial and axial flux generators. Both types have high efficiency and high power density. Recent studies have focused on axial flux permanent magnet (AFPM) generators. AFPM generators are considerable in terms of their high efficiency, high power density, and compact construction. Besides, the generators, with their high number of poles, are the most attractive solutions for direct drives in wind turbines [2, 3]. Despite the advantages of AFPM generators, AFPM generators have some disadvantages, such as cogging torque, which is a result of the interaction between the pole legs and slot edges (in the case of an unexcited stator and varying air-gap reluctance) [4].

The most common expression for the cogging torque is given in Equation (1).

$$T_{cog} = -\frac{1}{2}\phi_g^2 \frac{d\Re}{d\theta} \tag{1}$$

where ϕ represents the air-gap flux, $\Re$ the air-gap reluctance, and θ the angular position of the rotor.

The air gap reluctance changes periodically in Equation (1). Therefore, the Fourier series as given in Equation (2) can express the change of reluctance

$$T_{cog} = \sum_{k=1}^{\infty} T_{mk} \sin(mk\theta) \tag{2}$$

Received 3 May 2020, Accepted 9 July 2020, Scheduled 3 August 2020

* Corresponding author: Engin Hüner (engin.huner@klu.edu.tr).
The authors are with the Energy System Engineering Department, Kırklareli University, Kırklareli, Turkey.

where k is an integer value, m the least common multiple of the number of slots and poles, and T_{mk} a Fourier coefficient value. There are m periods for each mechanical revolution [5].

Slot opening is important in axial flux machine and leads to cogging torque so much in comparison with slot structure [6]. Also, the generated cogging torque in the AFPM synchronous generator with open-slotted creates harmonics form in the voltage curve [7].

In the literature, there are different types of methods that are given to reduce the cogging torque on the stator and rotor sides. These methods are more expensive than other methods. One of them is the change of slot structures on the stator side. In [8], soft magnetic wedges have been proposed as a low-cost method for reduction of cogging torque, in which soft magnetic wedges are used. The changes of the rotor side include using a different type of magnet, applying a different skew (conventional, hybrid, trapezoidal, triangular, dual-layer magnet step) to the magnets, magnet grouping, rotor shifting, and changing the magnet angle [9–13]. In this study, the magnets are rotated in their axes to decide the optimum angle for minimum cogging torque and maximum performance. Thus, the optimum harmonic distortion value for the best performance is investigated.

The generator with double flux morphology is also a well-known method for wind turbines. Besides, double flux morphology has both radial and axial magnetic fluxes [14]. Axial flux permanent magnet generators are suitable for direct drive due to their high number of poles. This generator type dose not require a reduction gear system compared with a traditional system. Thus, the losses due to the reduction gear system are eliminated, and efficiency increases [15].

In general, the conventional models for wind turbines consist of two stators and a rotor [16, 17] or two rotors and a stator. The dual-rotor system provides a balance for the existing axial forces in the stator. A double-rotor/single-stator structure in wind turbines (known as Torus-S) has high efficiency, low weight, and low volume [18]. In the case of using the rhomboidal winding structure, the number of poles increases. Also, trapezoidal and toroidal windings are used in the morphology of the double stator and single rotor. A toroidal winding has shorter end-winding rather than trapezoidal winding. Therefore, it has low winding resistance losses and high efficiency. The generators with a rotor and stator multi-disc structure are suggested for wind turbines and flow turbines [19, 20]. The magnetic reluctance does not change across the air-gap in the coreless structure of AFPM machines, which eliminates cogging torques [21–23]. The construction costs are also cheaper in the coreless axial flux machines [24]. Because of their simple construction and ease of manufacturing, they are also suggested as generators in wind turbines [25].

The value of the induced voltage is given in Equation (3) in the unloaded state [26].

$$E_{ph,n} = \sqrt{2} N_{ph} K_w \frac{f}{p} (Ro^2 - Ri^2) B_{n,e} \tag{3}$$

where $E_{ph,n}$ is the n_{th} values of induced voltage, N_{ph} the number of cycles per phase, K_w the winding factor, f the frequency value of the voltage, p the number of single poles, B_n the n_{th} value of the effective value of flux density, and R_o and R_i are the outer and inner radii of the stator.

In the case of an unloaded situation, the sinusoidal change of the induced voltage is given in Equation (4).

$$e_{ph}(wt) = \sum_n \sqrt{2} E_{ph,n} \sin(2\pi f t) \tag{4}$$

where w represents the angular velocity, and e_{ph} is the change of induced voltage depending on the angular velocity.

For the designed AFPM synchronous generator, Thd_V is the total harmonic distortion of the voltage, V_{Ln} the n_{th} values of the line voltage ($n = 5$, 7, 9, 11, 13, etc.), and V_{L1} the first value of the voltage harmonics in Equation (5).

$$Thd_V = \frac{\sqrt{\sum_n (V_{Ln})^2}}{V_{L1}} \quad (n = 5, 7, 9, 11, 13, \ldots) \tag{5}$$

This paper is regarding the effect of the magnet angle for an AFPM synchronous generator design. Especially, the effect of the magnet angle on the voltage and total current harmonics of the AFPM synchronous generator was investigated. Then, data sets were obtained from the experimental setup and magnetic analysis. In terms of the total harmonic distortion Thd, line voltage Uh, and cogging torque Tc values, the performance of the AFPM synchronous generator is evaluated.

2. MATERIAL AND METHODS

In this study, an AFPM synchronous generator was designed as a wind turbine. The magnetic analysis of AFPM synchronous generator was performed with ANSYS Maxwell Software according to the parameters given in Table 1. Then, the 3D analysis model of the AFPM synchronous generator was created based on the values given in Table 1. The magnetostatic analysis of the AFPM synchronous generator was realized to investigate the magnetic flux changes in the air gap.

Table 1. Physical dimension of design.

Parameter	Value
Stator Outer Diameter (Do)	210 [mm]
Stator Inner Diameter (Di)	130 [mm]
Output Power (S)	596 [VA] one rotor- one stator
Electromotor force (EMF)	147,4 [Volt]
Revolution per minute (n)	428 [rpm]
Inner diameter to outer diameter (λ)	0,619
Number of turns per slot (N_{ph})	80
Phase number	3
Slot number	42
Pole number	14
Winding Type	Toroidal
Maximum flux density in the stator core	1,8 Tesla
Magnet type	NdFeBr(N35) $40 \times 20 \times 10$ [mm]

Firstly, the air gap analysis was carried out to get minimum saturation at the edges of the slots and the highest magnetic flux density along the surface. Then, the changes in the RSPM placement angle were analyzed in terms of the performance of the generator.

The study flow chain is given Figure 1, which shows a general approach for the proposed model. The flow chain in Figure 1 shows the effect of the rectangle-shaped PM angle on cogging torque according to the magnetic analysis of the change of air gap. All analysis was realized by using ANSYS optimetric module. Then, the obtained results from the analysis were compared with the experimental ones. In this way, the analysis results were validated by experimental data that show the statistical parameters.

3. RESULTS OF ANALYSIS

The air gap from 1 mm to 10 mm was defined to analyze the magnetic flux density for the generator. In this study, all analysis studies were performed by Ansys Maxwell Finite Element Analysis Software. Especially, these analyses were realized in the magnetostatic analysis mode.

The full model is given in Figure 2(a). The magnetic flux distribution is shown in Figures 2(b) and 2(c) for 1 mm and 10 mm, respectively.

The magnetic flux peaks appeared at the edge of the slot for a 1 mm air gap. For a 1 mm air gap, the magnetic flux value in the slot edges is about 2.5 Tesla. In this study on axial flux generators, the average flux density of the air gap is chosen greater than 0.4 Tesla.

In Figure 2(b), the core is saturated at the slot edges for a 1 mm air gap (B_{ave} is higher than 1.8 Tesla). Furthermore, the analysis results show that for the 1 mm air gap, the average magnetic flux densities (B_{ave}) at the air gap and the core are 0.52843 Tesla and 0.78408 Tesla, respectively. For the 10 mm air gap, the average magnetic flux densities (B_{ave}) at the air gap and the core are 0.26764 Tesla and 0.36364 Tesla, respectively.

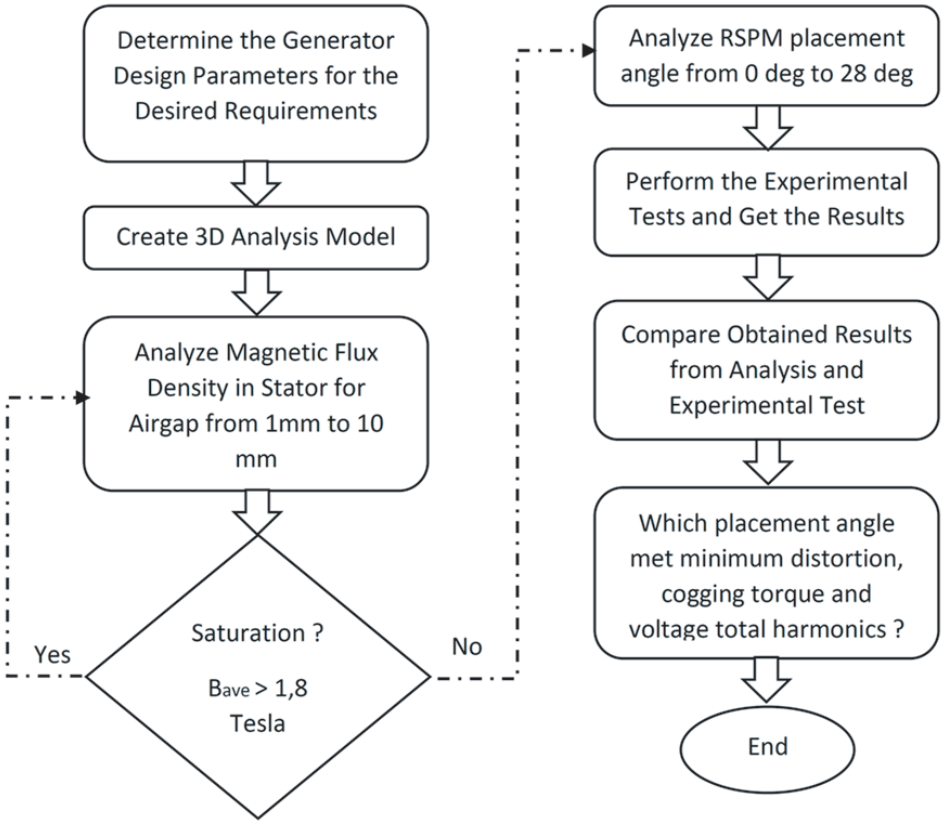

Figure 1. The study flow chain for analysis and experimental tests.

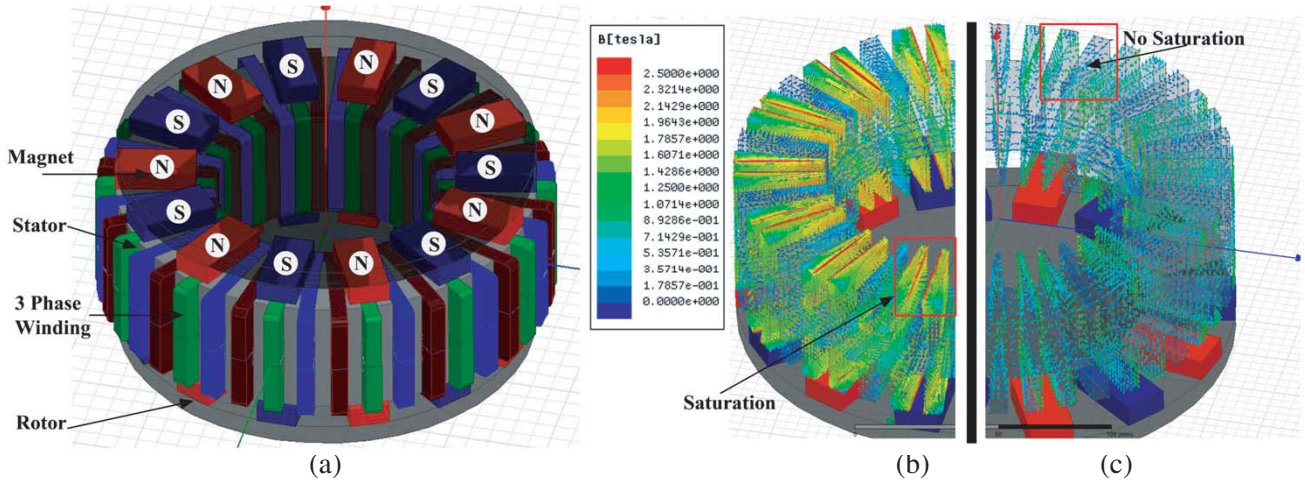

Figure 2. ANSYS Maxwell. (a) Full model. (b) Magnetic flux distribution 1 mm air gap. (c) Magnetic flux distribution 10 mm air gap.

With the magnetic flux density for the air gap from 1 mm to 10 mm, the analysis results show that 3 mm air gap provides minimum saturation at the edges of the slots and the highest magnetic flux density rate along the surface. The magnetic flux distribution for the 3 mm air gap is shown in Figure 3.

In Figure 3. for the 3 mm air gap, the average magnetic flux densities (B_{ave}) at the air gap and the core are 0.43402 Tesla and 0,65836 Tesla, respectively. According to these results, it is observed that

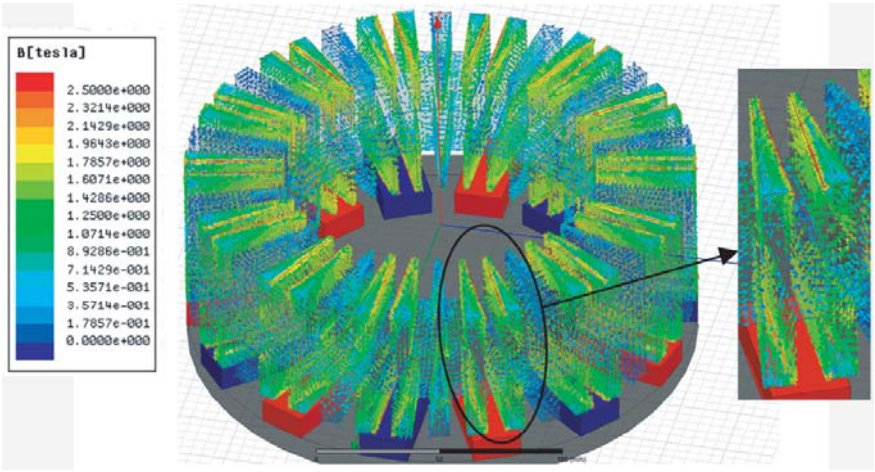

Figure 3. Magnetic flux distribution for 3 mm air gap.

minimum saturation is at the slot edges.

Besides, the design criteria shown in Figure 1 were provided at the 3 mm air gap. So, the minimum magnetic flux value meets the expectation ($B_{\text{ave}} > 0.4$ Tesla shown in Figure 1). Therefore, these results meet the desired requirements. Due to these results, a 3 mm air gap is considered for all further analyses.

The performance of the generator was investigated via a different magnet placement angle (from 0° to 28°). This angle range is considered for physical dimensions of RSPM.

Figure 4 shows magnetic flux distribution for the generator. In Figure 4(a), the magnetic flux distribution is shown at the PM angle with 0°, and in Figure 4(b), the magnetic flux distribution is shown at the RSPM angle with a 28° magnet angle.

In Figure 4(a), both of the stator's legs are affected by a magnet, while Figure 4(b) shows that the stator also has interaction on the third and fourth legs by a magnet. Hence, the spread of the interaction to the other legs provides a reduction effect on the cogging torque. The cogging torque is the sum of the individual torques of each pole [5].

In Figure 4(a), it is observed that a minimum one edge of the teeth and maximum two edges of the teeth were affected by a pole during the 360-degree movement of the rotor. In Figure 4(b), this effect is higher, so that minimum two-slot edges and maximum three-slot edges were affected by a pole during the 360-degree movement of the rotor. The higher effect on the slot edge by the permanent magnet provides a reduction on the cogging torque.

ANSYS optimetric module was used to realize the incremental change for the RSPM angle shown in Table 2 to observe the effect of angle change for the permanent magnet. Then, the obtained results shown in Table 2 for the average magnetic flux point out that the maximum change on the core for B_{ave}

Table 2. Average magnetic flux values for different pole angles.

Pole Angles	Average Magnetic Flux
0°	0.6584
4°	0.6596
8°	0.6585
12°	0.6568
16°	0.6508
20°	0.6459
24°	0.6400
28°	0.6341

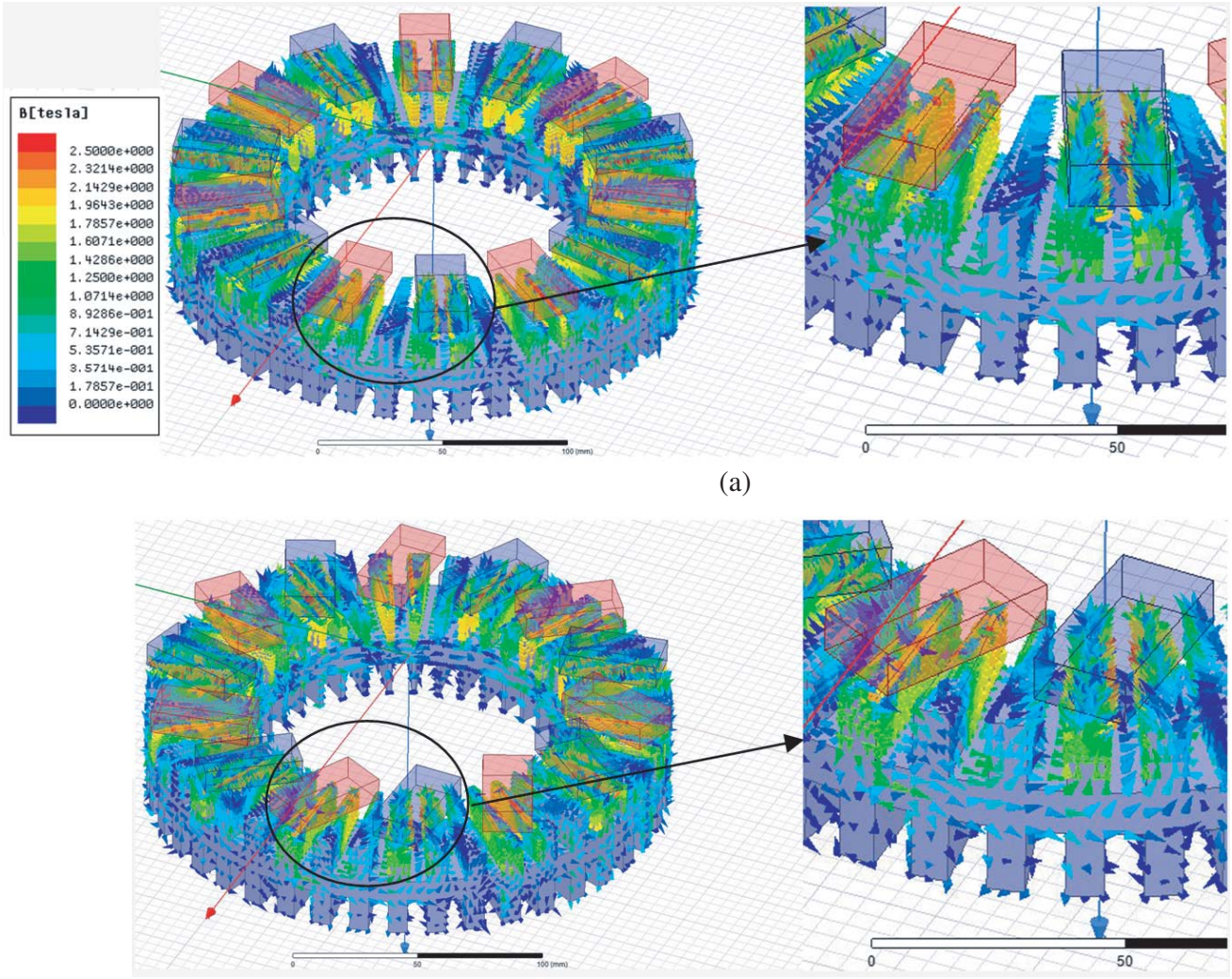

Figure 4. Magnetic flux distribution. (a) PM angle with 0°. (b) PM angle with 28°.

is 3.67%. However, the magnetic poles interact on a wider iron core surface depending on the magnet angle, which shows that the cogging torque decreases.

Therefore, due to the magnetic flux distribution, the decline in power will also be lower.

For the RSPM angle with 20°, the magnetic flux distribution is shown in Figure 5. According to the obtained results from the analysis, the average magnetic flux density (B_{ave}) is 0.6459 Tesla.

The analysis results for the cogging torque depending on the permanent magnet angle are shown in Figure 6. The obtained results show that the permanent magnet angles with 4°, 8°, 12°, 16°, 20°, 24°, and 28° provide the reduction on the cogging torque by 8.14%, 23.82%, 42.29%, 63.47%, 81.22%, 94.61%, and 96.26% compared with 0° rectangular-shaped permanent magnet angle.

4. EXPERIMENTAL SETUP OF THE AFPM SYNCHRONOUS GENERATOR

One of the most important disadvantages of the AFPM synchronous generators is the open slot structure, which leads to increasing the cogging torque. High cogging torque causes harmonics in the output voltage waveform. The effect of the RSPM placement angle for the generator was investigated to overcome high harmonics and cogging torques. The proposed method is regarding rotating the rectangular magnet on its axis. As a result of the magnetic analysis, changing the magnet angle has reduced the total power.

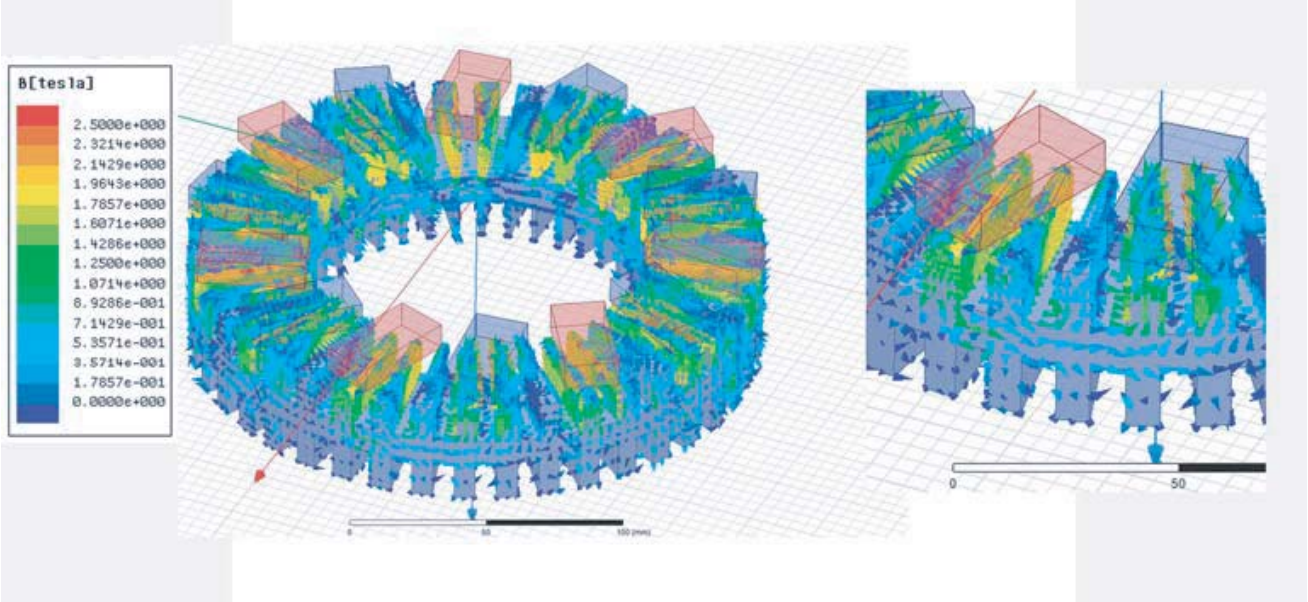

Figure 5. Magnetic flux distribution PM angle with 20°.

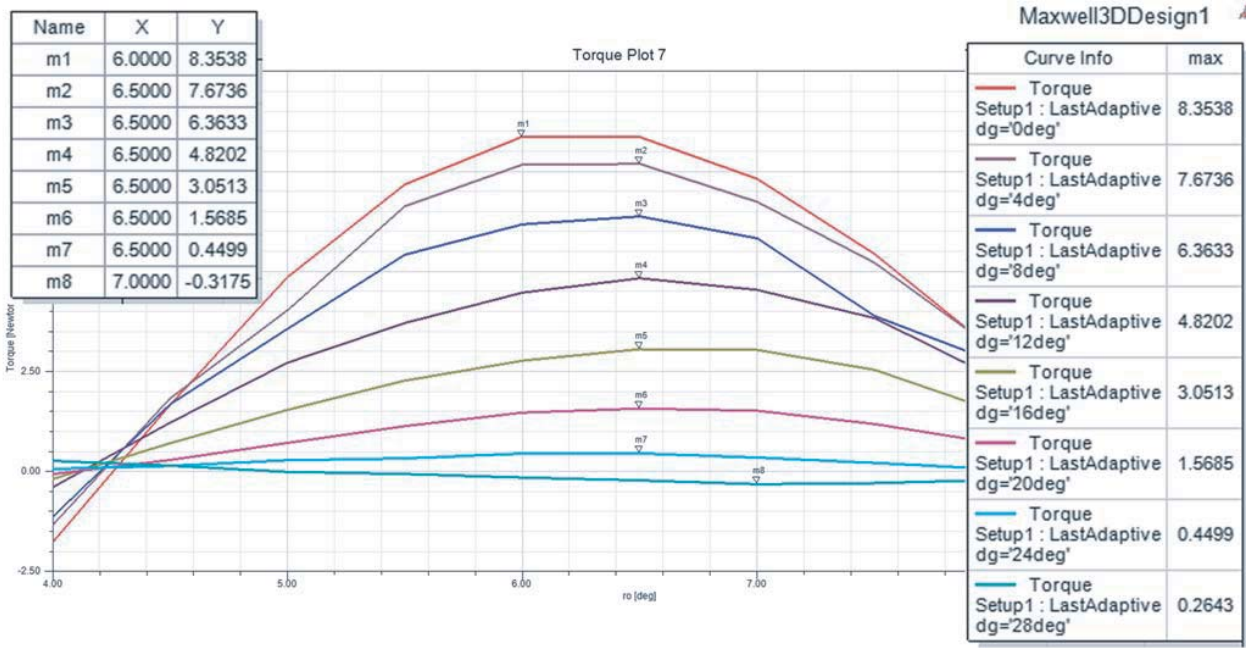

Figure 6. Cogging torque analysis for RSPM angles.

As a result of the magnetic analysis, changing the magnet angle has reduced the total power because of interaction on a wider surface. Hence, it reduces the cogging torque. The magnet-holder apparatus is shown in Figure 7(a), which was designed to adjust the magnets to the desired angle value. In Figure 7(b), the magnets are mounted on the rotor iron with the aid of snap rings, so that the magnets can move freely on the iron rotor surface.

Plexiform with the rotor is given in Figure 8(a). Plexiform helps to fix the desired magnet rotation angle. The designed stator with three-phase toroidal windings is given in Figure 8(b).

Figure 9 shows the experimental setup of the AFPM synchronous generator. The experimental

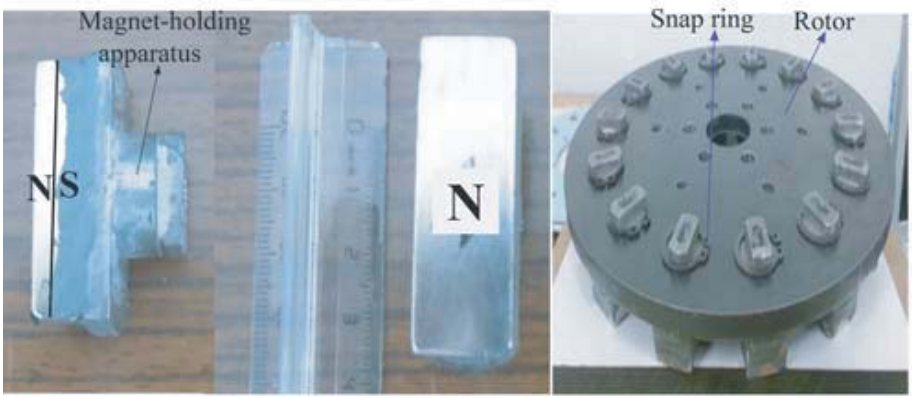

(a) (b)

Figure 7. Rotor. (a) Magnet-holding apparatus. (b) Rotor with magnet.

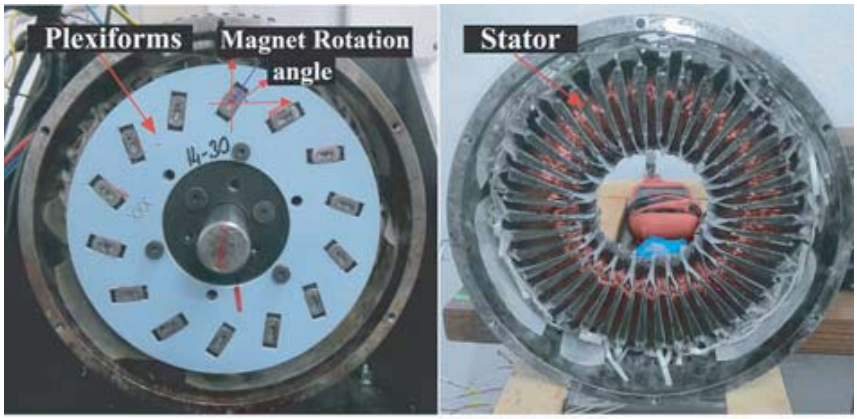

(a) (b)

Figure 8. Designed test generator. (a) Plexiforms with rotor. (b) Stator.

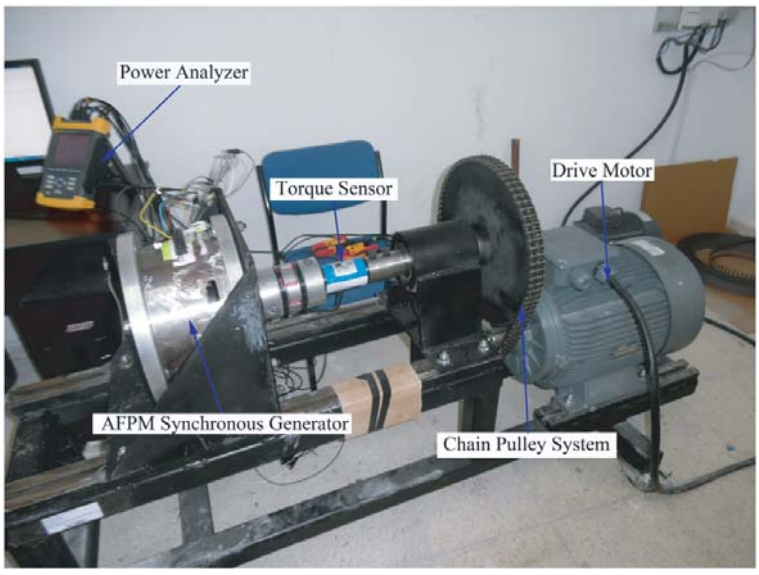

Figure 9. Experimental setup of the AFPM synchronous generator.

setup consists of an asynchronous motor, which contains a drive machine, a torque sensor, an inverter, a power analyzer, and a computer. A 22 kW asynchronous motor in the experimental setup was used as a drive machine. The chain system in the experimental setup reduces the speed of the drive machine. A 8645 model torque sensor is connected to the test generator by coupling to measure the cogging torque. The speed of the drive machine is adjusted with an ABB ACS850 drive and a USB connection kit to obtain the desired generator output frequency. In the experiments, the output voltage curves and harmonic values were taken at the constant frequency with the Fluke 434 Power Analyzer.

4.1. Open Circuit Experiment

The results obtained from the power analyzer in the experimental setup shown in Figure 9 are given in Figures 10–13. All of the measurements were made by taking the values of the open-circuit voltage at a frequency of 50 Hz. Figure 10(a) shows the three-phase output voltage curve of the AFPM synchronous generator. The total harmonic distortion was about 8.9% in Figure 10(b), and the line voltage between phases was 147.4 volts. The fifth harmonic level was high considering the experimental data.

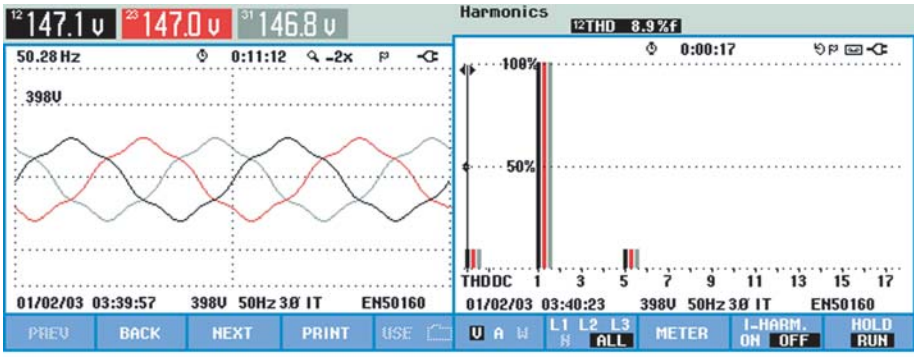

(a) (b)

Figure 10. AFPM synchronous generator at 0° magnet angle. (a) Output voltage curve. (b) Thd values.

Figure 11 shows the results for a 20° magnet angle. The output voltage of 143.5 volts and total harmonic distortion (Thd) at 5.2% of voltage were obtained and shown in Figure 11(a) and Figure 11(b). Compared with the 0° magnet angle, output voltage and Thd decreased by 2.6% and 41.6%, respectively. The output voltage curve changed slightly at 20°, but the total harmonic distortion was significantly reduced.

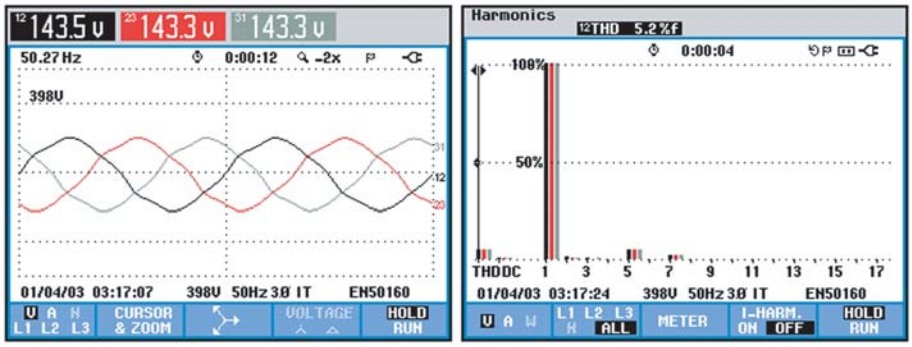

(a) (b)

Figure 11. AFPM synchronous generator at 20° magnet angle (a) Output voltage curve (b) Thd values.

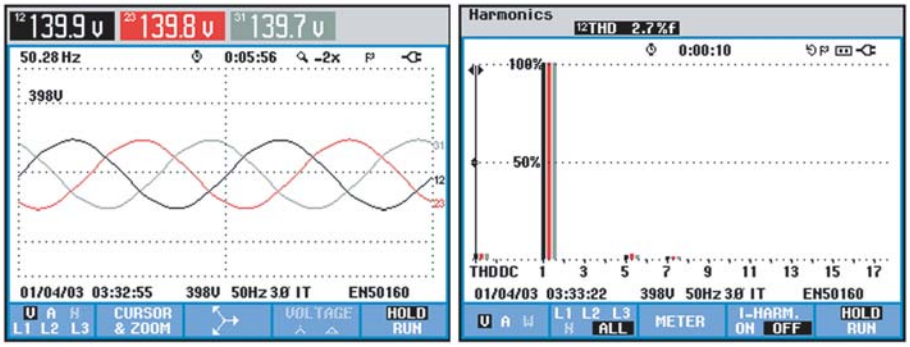

(a) (b)

Figure 12. AFPM synchronous generator at 28° magnet angle. (a) Output voltage curve. (b) Thd values.

Figure 12 shows the results for a 28° magnet angle, which was the maximum physical limit in our design. In the unloaded state, the output voltage and Thd values were 139.8 volts and 2.7%, respectively. Compared to the 0° magnet angle, the output voltage and Thd decreased by 4.96% and 69.7%, respectively.

The obtained results from the experimental setup are shown in Table 3. Compared to the 0° magnet angle, the percentage change in the cogging torque values at 20° and 28° were 71.4% and 85.7%, respectively. Therefore, when being evaluated together with the other parameters, a 20° magnet angle meets the desired requirement (minimizing) in terms of cogging torque.

Table 3. Experimental data by magnet angle.

Magnet Angle (Mag°)	Uh (Voltage)	Thd (%)	T_C (Nm)
0°	147.1	8,9	7
4°	147.8	9,1	6
8°	146.5	8,4	5
12°	146.7	7,7	4
16°	144.8	6,3	3
20°	143.3	5,2	2
24°	142.7	4,4	1,5
28°	139.8	2,7	1

The change of the harmonic distortion by the magnet angle of the AFPM synchronous generator is shown in Figure 13(a), and Figure 13(b) shows the change of cogging torque. The usage of the AFPM synchronous generators shows that the proposed method seems useful for Thd and cogging torque.

4.2. Loaded Operation

Six-step winding resistance was used for the loaded operation. The measurements were obtained without changing the reference points. The resistance level was 60.5 ohm.

4.2.1. Harmonic Values

The generated current and voltage harmonics at different magnet angles were observed. The generated harmonic values were recorded by increasing the magnet angles from 0° to 28°.

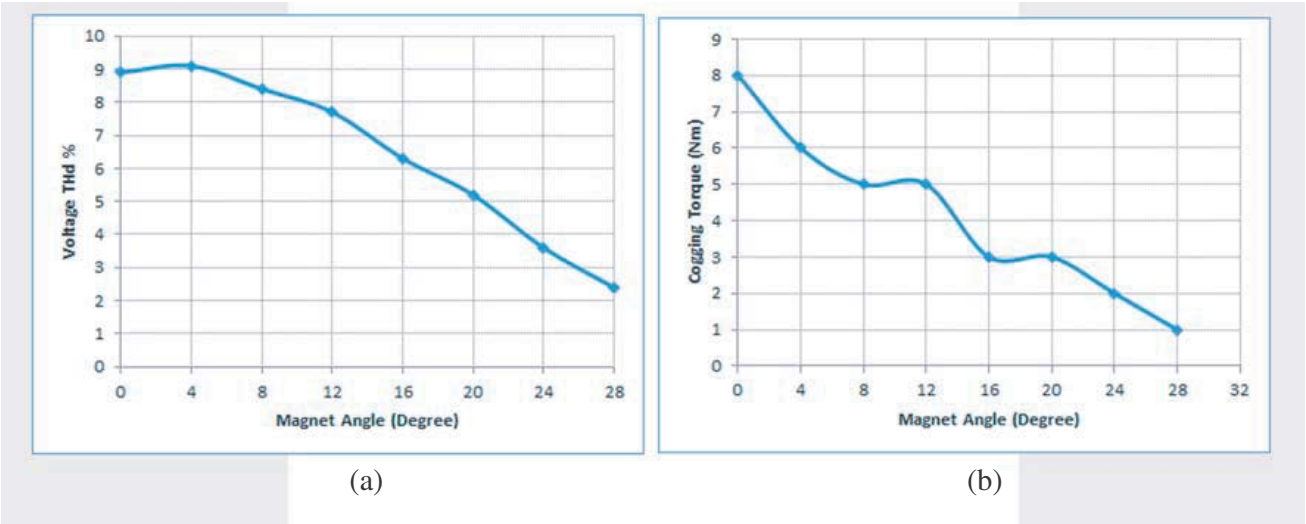

Figure 13. AFPM synchronous generator due to magnet angle. (a) Percentage change in voltage harmonics. (b) Cogging torque.

Figure 14 shows that in the results for the 0° magnet angle, the generator produced 7.4% Thd voltage (Thd_V), and 7.6% Thd current (Thd_I) when the 60.5 ohm load resistance was loaded. When the magnets were at angles 12°, 20°, and 28°, the voltage harmonics were reduced by 27%, 53%, and 76%, respectively, compared to at 0°. Compared to the harmonic distortion generated at 0°, the total harmonic distortion of the current was similarly reduced by 26%, 52%, and 74% at 12°, 20°, and 28°, respectively.

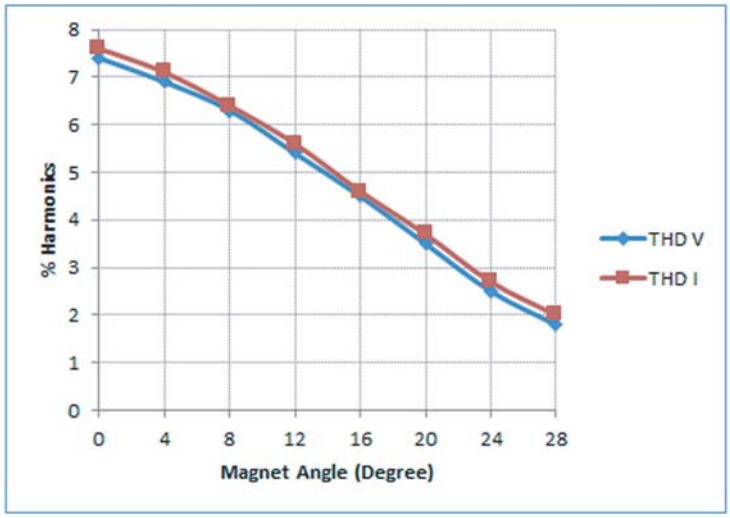

Figure 14. Thd_V and Thd_I curves at the first-stage load (at different magnet angles).

4.2.2. Voltage Values

The voltage waveforms were obtained from the experimental setup to investigate the performance of the generator for the RSPM placement angles. The generator output voltage decreases as the current of the generator is increased. In this experiment, the magnet angles were increased under 60.5 ohm load resistance, and the obtained line voltages are given in Table 4.

Table 4. Experimental result in the loaded state.

M. Deg	0°	4°	8°	12°	16°	20°	24°	28°
Load resistance 60.5 ohm								
Thd_V	7,4	6,9	6,3	5,4	4,5	3,5	2,5	1,8
Thd_A	7,6	7,1	6,4	5,6	4,6	3,7	2,7	2
I_out	1,3	1,3	1,3	1,28	1,26	1,25	1,2	1,2
S (VA)	300.2	298.6	297.5	273.2	271.5	269.6	267.8	263.2
R	133.5	132.8	132.3	131.6	130.8	129.9	129.0	126.8
S	133.4	132.8	132.3	131.6	130.8	129.9	129.0	126.8
T	133.3	132.7	132.3	131.5	130.7	129.8	129.0	126.7

Experimental results in Table 4 include the total harmonic distortion for voltage (Thd_V), total harmonic distortion for current (Thd_I), output current (I_out), apparent power (S), and phase voltage (R, S, T) according to a mechanical degree.

Figure 15 shows that the generator produced a line voltage (U_line) at each phase of 133 volts at 60.5 ohm load resistance and a constant frequency of 50 Hz with a 0° magnet angle. Under the same load, compared to the 0° phase-to-phase voltage, the voltage losses were 2.6% and 5.7% at magnet angles of 20° and 28°, respectively.

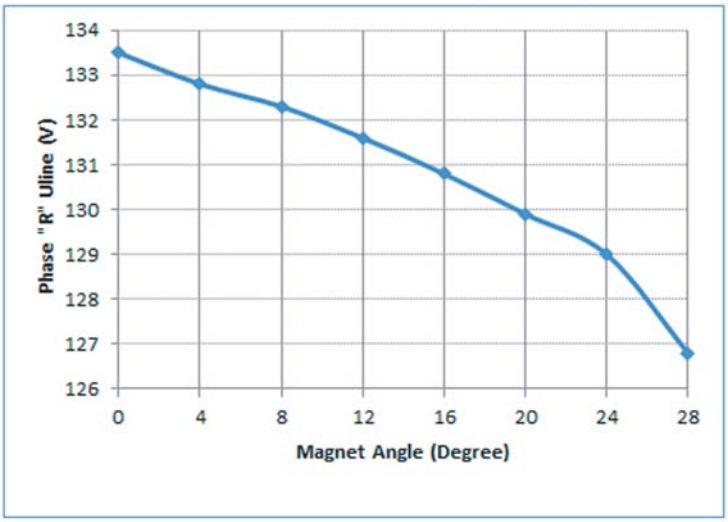

Figure 15. U_line voltage curves produced at different magnet angles (Load resistance is 60.5 ohm).

4.2.3. Apparent Power Values

The apparent power (S_line) for each phase was obtained from the experimental setup for the RSPM placement angles from 0° to 28°.

Regarding the output of the generator, in the case of 60.5 ohm, the generator produced 1.5 A current per phase under constant 50 Hz frequency.

The magnet angles were increased at 60.5 ohm load resistance, then the line voltage and current values were obtained, and S_line values were calculated.

Figure 16 shows that the generator produced an average of 301 VA in 60.5 ohm load resistance and at the constant frequency for 0° magnet. Under the same load, compared to S_line at 0°, 10.2% and 13.1% of power were lost at magnet angles of 20° and 28°, respectively.

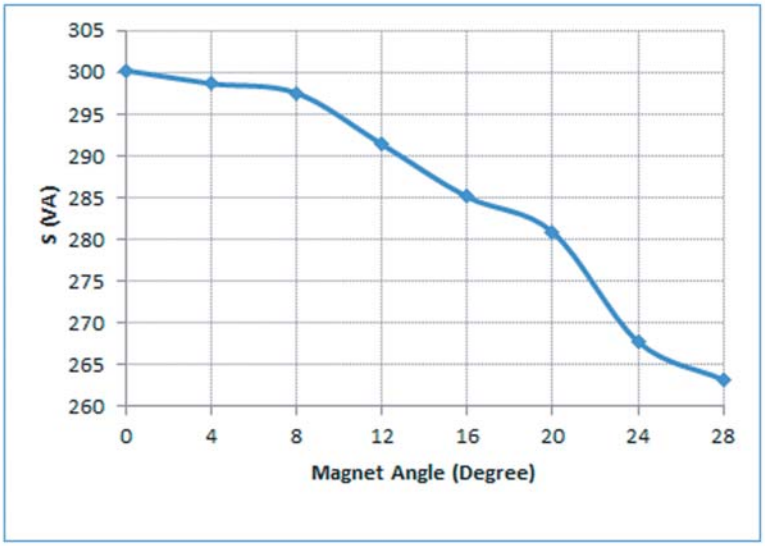

Figure 16. S-line apparent power produced at different magnet angles (Load resistance is 60.5 ohm).

4.2.4. Statistical Analysis of Results

In this study, the experimental results and analysis results were compared in Table 5. The cogging torques of simulated and experimental results are S_Tc and E_Tc respectively, which are shown in Table 5. Also, % S_Tc and % E_Tc represent the percentage of S_Tc and E_Tc. As the placement angle of RSPM was changed from 0 to 28 degrees, the cogging torque decreases. The results shown in Table 5 show the higher convergence between analysis and experimental results, which (S_Tc, E_Tc) are correlated by 0.997432189.

Table 5. Comparisons results from test and analysis studies.

	Simulation Results		Experimental Results	
	S_Tc	% S_Tc	E_Tc	% E_Tc
0	8,3538	0	7	0
4	7,6736	0,081424023	6	0,142857143
8	6,3633	0,238274797	5	0,285714286
12	4,8202	0,422993129	4	0,428571429
16	3,0513	0,634741076	3	0,571428571
20	1,5685	0,812241136	2	0,714285714
24	0,4499	0,94614427	1,5	0,785714286
28	0,3117	0,962687639	1	0,857142857
S_Tc average		0,585500867	E_Tc average	0,540816286
S_Tc std		0,348146867	E_Tc std	0,247014787
S_Tc, E_Tc Correlation			0,997432189	

5. CONCLUSION

In this study, the power quality of an AFPM synchronous generator used in wind turbines was experimentally analyzed. As a result, the magnetic analysis for AFPM synchronous generator under different RSPM angles was realized at ANSYS Maxwell. Besides, the experimental studies were performed to validate and compare with the analysis results. In the case of a 20° permanent angle, the obtained results show that Thd and Tc are improved by 41.6% and 71.4%, respectively. Furthermore, U_{h} and S_{line} were decreased by 2,6% and 10.2%, respectively. Therefore, for minimum Thd-Tc and maximum power, the optimum angle is found by 20° compared with other angles. Thus, the maximum performance was obtained from AFPM synchronous generator with an optimum angle by using a rectangular type NdFeB magnet in this study. Also, a cheaper and easier method has been proposed according to cogging torque reducing techniques compared with skew methods that need special magnet shapes for the rotor side, and it has been proven both in magnetic analysis and experimental results.

ACKNOWLEDGMENT

This work was supported by Kırklareli University on Scientific Research Commission, Project Number: KLUBAP-039.

REFERENCES

1. Demir, U. and M. C. Aküner, "Design and analysis of radiaxial induction motor," *Electr. Eng.*, Vol. 100, 2361, 2018, https://doi.org/10.1007/s00202-018-0708-6.
2. Pantea, A., A. Yazidi, F. Betin, G. A. Capolino, and V. Lanfranchi, "Six-phase axial flux permanent magnet generator model: simulation and experimental validation," *IEEE 25th International Symposium on Industrial Electronics*, 192–197, June 2016, doi: 10.1109/ISIE.2016.7744888.
3. Patel, N. and N. Uddin, "Design and performance analysis of a magnetically levitated vertical axis wind turbine based axial flux pm generator," *IEEE 7th International Conference on Electrical and Computer Engineering*, Dhaka, Bangladesh, December 20–22, 2012, doi: 10.1109/ICECE.2012.6471657.
4. Zhu, Z. Q. and D. Howe, "Influence of design parameters on cogging torque in permanent magnet machines," *IEEE Transactions on Energy Conversion*, Vol. 15, No. 4, 407–412, December 2000, doi: 10.1109/60.900501.
5. Dosiek, L. and P. Pillay, "Cogging torque reduction in permanent magnet machines," *IEEE Transaction on Industry Applications*, Vol. 43, No. 6, 1565–1571, 2007.
6. Reza, M. M., A. Ahmad, P. Kumar, and R. K. Srivastava, "Semi-analytical model for triangular skewed permanent magnet axial flux machine," *IEEE Transportation Electrification Conference*, 1–5, 2017, doi: 10.1109/ITEC-India.2017.8333843.
7. Aycicek, E., N. Bekiroglu, and S. Ozcira, "An experimental analysis on cogging torque of axial flux permanent magnet synchronous machine," *Proc. Natl. Acad. Sci., India, Sect. A Phys. Sci.*, Vol. 86, No. 1, 95–101, 2016, doi: 10.1007/s40010-015-0235-z.
8. Kumar, K. and R. K. Srivastava, "Cost-effective stator modification techniques for cogging torque reduction in axial flux permanent magnet machines," *IEEE Transportation Electrification Conference and Expo*, 1–6, November 2018, doi: 10.1109/IAS.2018.8544690.
9. Aydin, M., Z. Q. Zhu, T. A. Lipo, and D. Howe, "Minimization of cogging torque in axial-flux permanent-magnet machines: design Concepts," *IEEE Transactions on Magnetics*, Vol. 43, No. 9, 3614–3622, 2007, doi: 10.1109/TMAG.2007.902818.
10. Choi, J. H., J. H. Kim, D. H. Kim, and Y. S. Baek, "Design and parametric analysis of axial flux pm motors with minimized cogging torque," *IEEE Transaction on Magnetics*, Vol. 45, No. 6, 2855–2858, 2009, doi: 10.1109/TMAG.2009.2018696.
11. Hsieh, M. F., D. G. Dorrell, Y. H. Yeh, and S. Ekram, "Cogging torque reduction in axial flux machines for small wind turbines," *35th Annual Conference of IEEE Industrial Electronics*, 4435–4439, Porto, Portugal, November 2009, doi: 10.1109/IECON.2009.5414896.

12. Demir, U. and M. C. Aküner, "Using taguchi method in defining critical rotor pole data of LSPMSM considering the power factor and efficiency," *Tehnički Vjesnik*, Vol. 24, No. 2, 347–353, 2017, DOI: 10.17559/TV-20140714225453.
13. Huang M. S., P. C. Chen, Y. S. Huang, and K. C. Chen, "Reduce the cogging torque of axial flux permanent magnet synchronous motor for light electric vehicle applications," *IEEE International Conference on Industrial Technology*, 193–197, Taipei, Taiwan, 2016, doi: 10.1109/ICIT.2016.7474749.
14. Gor, H. and E. Kurt, "Waveform characteristics and losses of a new double sided axial and radial flux generator," *International Journal of Hydrogen Energy*, Vol. 41, 2512–12524, 2015, doi:10.1016/j.ijhydene.2015.12.172.
15. Azzouzi, J., N. A. Karim, G. Barakat, and B. Dakyo, "Axial flux pm synchronous generator design optimization: robustness test of the genetic algorithm approach," *European Conference on Power Electronics and Aplplications*, September 11–14, 2005, doi: 10.1109/EPE.2005.219630.
16. Parviainen, A., M. Niemela, and J. Pyrhönen, "A novel axial flux permanent magnet machine to laboratory use," *Computer Engineering in Applied Electromagnetism*, 333–336, 2005, doi: 10.1007/1-4020-3169-6_58.
17. Belicova, E. and V. Hrabovcova, "Analysis of an axial flux permanent magnet machine (AFPM) based on coupling of two seperated simulation models (electrical and thermal ones)," *Journal of Electrical Engineering*, Vol. 58, No. 1, January 3–9, 2007.
18. Taran, N. and M. Ardebili, "A Novel approach for efficiency and power density optimization of an axial flux permanent magnet generator through genetic algorithm and finite element analysis," IEEE 23th International Symposium on Industrial Electronics, Istanbul, Turkey, June 2014, doi: 10.1109/ISIE.2014.6864699.
19. Zhang, Z., R. Nilssen, S. M. Muyeen, A. Nysveen, and A. Al-Durra, "Design optimization of ironless multi stage axial flux permanent magnet generators for offshore wind turbines," *Engineering Optimization*, Vol. 49, 815–827, May 2015, doi: 10.1080/030525X.2016.1208191.
20. Keysan, O., S. A. McDonald, and M. Mueller, "A direct drive permanent magnet generator design for a tidal current turbine (seagen)," *IEEE International Electric Machines & Drives Conference, IEMDC*, Niagara, Falls, ON, Canada, May 2011, doi: 10.1109/IEMDC.2011.5994850.
21. Virtic, P., M. Vrazic, and G. Papa, "Design of an axial flux permanent magnet synchronous machine using analytical method and evolutionary optimization," *IEEE Transactions on Energy Conversion*, Vol. 31, No. 1, 150–158, March 2016, doi: 10.1109/TEC.2015.2477319.
22. Demir, U. and M. C. Aküner, "Design and optimization of in-wheel asynchronous motor for electric vehicle," *Journal of the Faculty of Engineering and Architecture of Gazi University*, Vol. 33, No. 4, 1517–1530, 2018, DOI: 10.17341/gazimmfd.416448.
23. Rallabandi, V., N. Taran, and D. M. Ionel, "Multilayer concentrated winding for axial flux pm machines," *IEEE Transactions on Magnetics*, Vol. 53, No. 6, June 2017, doi: 10.1109/TMAG.2017.2661312.
24. Daghigh, A., H. Javadi, and H. Torkaman, "Design optimization of direct-coupled ironless axial flux permanent magnet synchronous wind generator with low cost and high annual energy yield," *IEEE Transactions on Magnetics*, Vol. 52, No. 9, September 2016, doi: 10.1109/TMAG.2016.2560143.
25. Zhang, Z., A. Matveev, R. Nilssen, and A. Nysveen, "Ironless permanent magnet generators for offshore wind turbines," *IEEE Transactions on Industry Applications*, Vol. 50, No. 3, May/June 2014, doi: 10.1109/TIA.2013.2289983.
26. Ayat, Y. S. and M. R. A. Pahlavani, "3D Computation of no-load magnetic flux density in slotless axial-flux permanent magnet synchronous machines using conformal mapping," *IET Electric Power Applications*, Vol. 11, No. 8, 1391–1396, September 2017, doi: 10.1049/iet-epa.2016.0772.